

Supplementary Experimental Methods

Chemicals. MoB powder (~325 mesh, 99.5%) was purchased from Sigma-Aldrich Chemical Cor. (St. Louis, USA), and stored in an argon-filled glove box. Melamine (C₃H₆N₆, 99%) and potassium hydroxide (KOH, 95%) were purchased from Aladdin Industrial Inc. (Shanghai, China). All the chemicals were used without further purification. Deionized water was used throughout the whole experiment.

Synthesis of *g*-C₃N₄ powder. *g*-C₃N₄ powder was prepared by thermal polymerization of melamine under high temperature. In details, 10 g of melamine was placed in a ceramic crucible and heated at 550 °C for 4 h in a tube furnace at a ramp rate of 5 °C min⁻¹ under argon atmosphere. After being cooled down to room temperature, the obtained yellow solid was collected and fully ground, yielding the powder samples (denoted as *g*-C₃N₄).

Synthesis of MoB/*g*-C₃N₄ Schottky catalyst. A series of MoB/*g*-C₃N₄ Schottky catalysts were prepared by physical mixing, kneading and grinding of different weight ratio of commercial MoB and *g*-C₃N₄ powders in an agate mortar.

Characterization. Phase identification was performed by a Bruker AXS D8 Advance powder X-ray diffractometer (Bruker, Germany) using Cu K α radiation ($\lambda = 1.5418 \text{ \AA}$), in a 2θ angular range of 20-60° with a velocity of 0.02° in 4 s. Temperature-dependent resistivity plots were recorded in the temperature range from 20 to 300 K in steps of 5 K using a Keithley 4200-SCS semiconductor analyzer (Keithley, USA) by a standard four-probe method. To determine the C/N molar ratio, X-ray photoelectron spectroscopy were performed on an ESCALAB 250 Xi spectrometer (VG Scientific Co., UK) with an Al K α X-ray radiation (1486.6 eV) for excitation, and otherwise elemental combustion analysis was accomplished using an Elementar Vario Micro Cube system (Hanau, Germany). Ultraviolet–visible absorption spectra were measured on a Lambda 35 spectrometer (Perkin–Elmer Instruments, USA). Geometric morphology and element distribution were divulged by JEOL JSM-7100F scanning electron microscope (JEOL, Japan) coupled with an Oxford IE250 energy-dispersive X-ray spectrometer (Oxford Instruments, UK). Energy-loss near-edge structure spectra were obtained using a Hitachi HF-2000 field-emission transmission electron microscope (Hitachi, Japan) operating at 200 kV, equipped with a cold field emission gun and a Gatan PEELS 666 parallel electron spectrometer (Gatan Inc., USA). Steady-state photoluminescence spectra were measured on a FluoroLog3-21 spectrofluorimeter (HORIBA Jobin Yvon, France) with the excitation light at 325 nm. Ultraviolet photoemission spectroscopy was also carried out on an ESCALAB 250 Xi spectrometer using He I resonance lines (21.2 eV).

Electrochemical measurements. All HER measurements were performed on a CHI 760D electrochemical workstation (Chenhua, China), using a five-necked glass cell containing rotating disk working electrode, saturated calomel reference (SCE) electrode, and graphite rod counter electrode (Pine Instrument Co., USA). The electrodes were prepared by drop-casting catalyst inks including catalyst powders onto a polished glassy carbon electrode (0.196 cm²), and the electrode surface was finally loaded with HER catalyst of 0.25 mg_{cat}/cm_{disk}² and a mass ratio of 5:5:1 of catalyst to carbon Vulcan XC72R to Nafion. The as-prepared electrodes were tested in 1 M KOH or 0.5 M H₂SO₄ solution after several repeated cyclic voltammeteries for electrochemical surface activation. Polarization curves were recorded by linear sweep voltammetry with a scan rate of 5 mV/s under an electrode rotation rates of 1 600 rpm for gas diffusion, and then replotted as overpotential (η) versus log current (log j) to obtain the Tafel plots. The Nyquist plots were measured with frequencies ranging from 100 kHz to 0.1 Hz at an overpotential of 150 mV. All the potentials were calibrated to a reversible hydrogen electrode (RHE). *IR* drop correction was used in all the experiments.

DFT computations. A periodic slab model of the MoB (112)-p(3 × 2) surface consisting of 14 Å × 17 Å slab and a 18 Å vacuum layer was used to compute the electronic structure and electrochemical mechanism of HER at the atomic and molecular level. The bottom 132 Mo and B atoms were frozen while the remaining atoms (from 108 to 259) were allowed to relax without constraint. Another periodic slab model of the g-C₃N₄ (001)-p(1 × 1) surface consisting of a 13 Å × 23 Å slab and a 18 Å vacuum thickness was constructed. Three layers of water with ~50 H₂O molecules were introduced inside the vacuum layer to simulate the electrical double layer formation during cathodic HER. The initial geometric structures were relaxed to a local minimum, and an *ab initio* molecular dynamic (AIMD) simulation was carried out to equilibrate the interaction between water molecules and the interface using the CP2K package.^[1] We used Nose-Hoover thermostat to sample the canonical ensemble.^[2] The relatively short timescales of AIMD limit the sampling step size to 1.0 fs; therefore, simulations were run for 10 ps. For rapidly exploring a large volume of phase-space volume of water network configurations without destroying the hydrogen bonding, a statistical sampling temperature of 300 K was chosen. The generalized-gradient approximation (GGA), as parameterized by Perdew, Burke and Ernzerhof,^[3] was utilized to compute the exchange-correlation energy. Dispersion interaction was considered in calculations by using empirical parameterized Grimme (D3) method.^[4] The elemental valence electrons were described using hybrid Gaussian and plane-wave basis sets, and the cutoff energy of 500 Rydberg of auxiliary plane-wave basis sets were adopted. We employed special double- ζ valence plus polarization basis sets optimized to minimize the basis set superposition errors. Core electrons were described with the norm-conserving and separable Goedecker-Teter-Hutter pseudopotentials.^[5] Brillouin zone integration was performed in reciprocal space, with the k-space sampling at the gamma point only. Transition states were investigated using climbing image nudged-elastic-band method (CI-NEB) with convergence criterion of 0.05 eV/Å.^[6]

Supplementary Figures

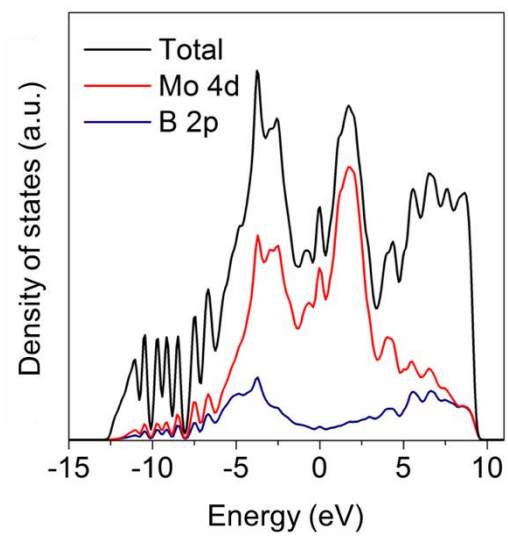


Figure S1. Total DOS and PDOS onto Mo 4d, and B 2p states for pure MoB.

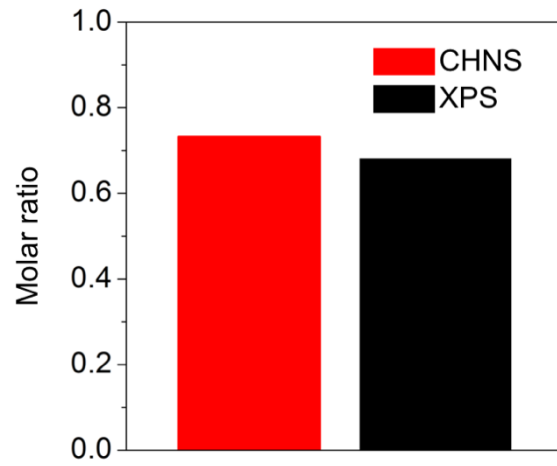


Figure S2. C/N molar ratios of *g*-C₃N₄ powders obtained by CHNS and XPS analysis.

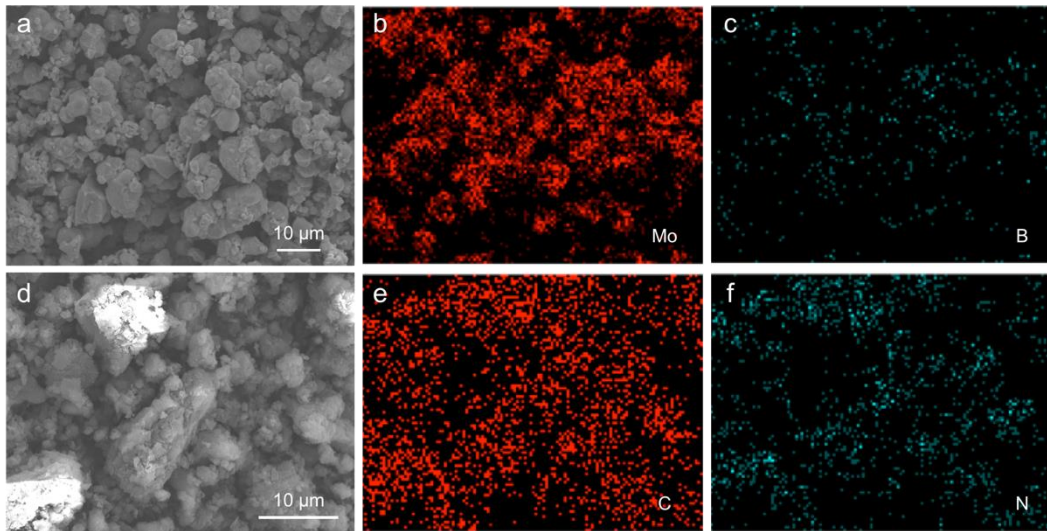


Figure S3. (a, d) SEM images and (b, c, e, f) SEM-EDS images of pristine MoB (a–c) and *g*-C₃N₄ powder (d–f).

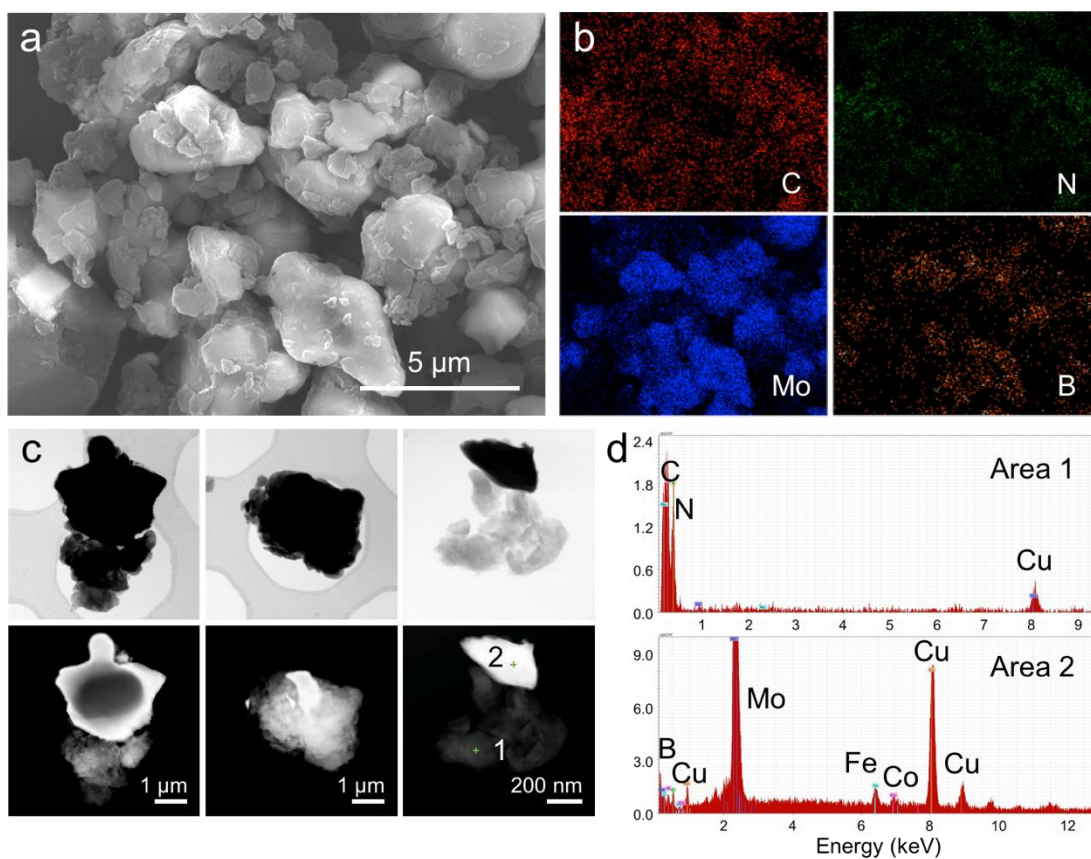


Figure S4. (a) SEM image, (b) SEM-EDS mapping images, (c) TEM images, and (d) EDS spectra of MoB/g-C₃N₄ Schottky catalyst.

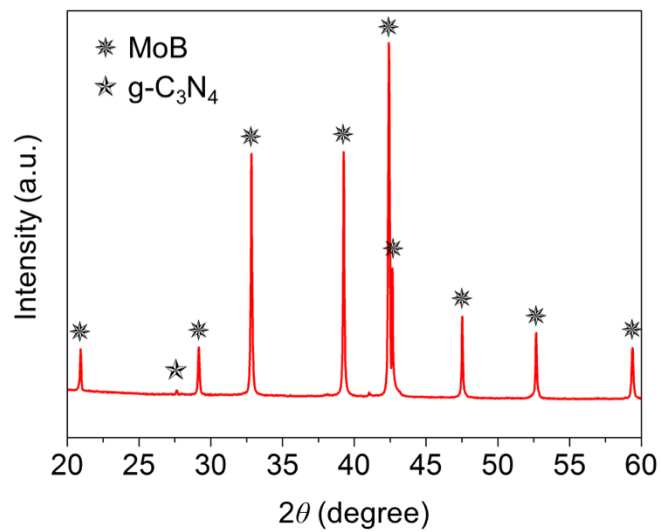


Figure S5. XRD pattern of MoB/g-C₃N₄ Schottky catalyst.

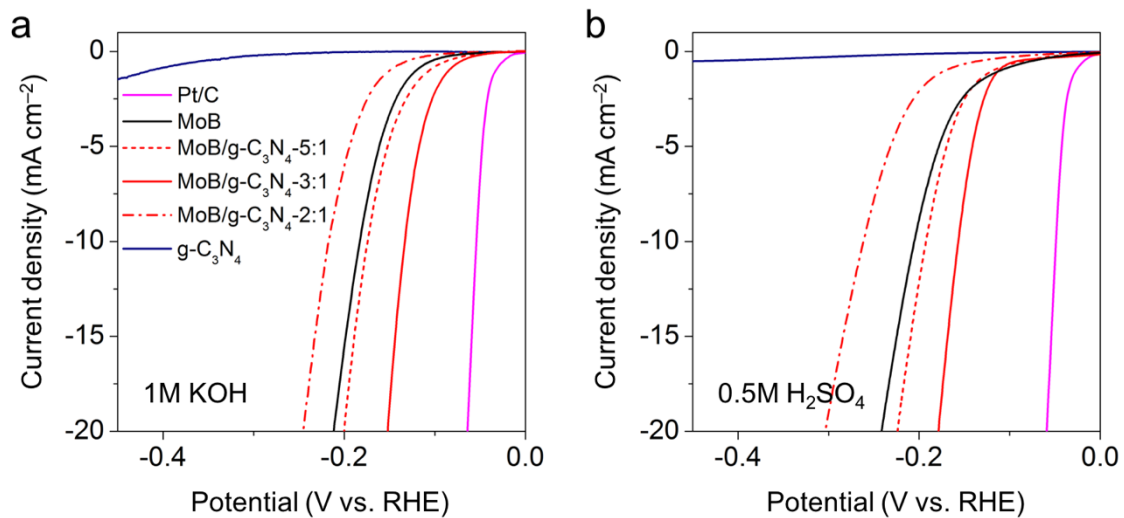


Figure S6. LSV polarization curves of MoB/g-C₃N₄ Schottky catalysts with different weight ratios in (a) 1 M KOH and (b) 0.5 M H₂SO₄.

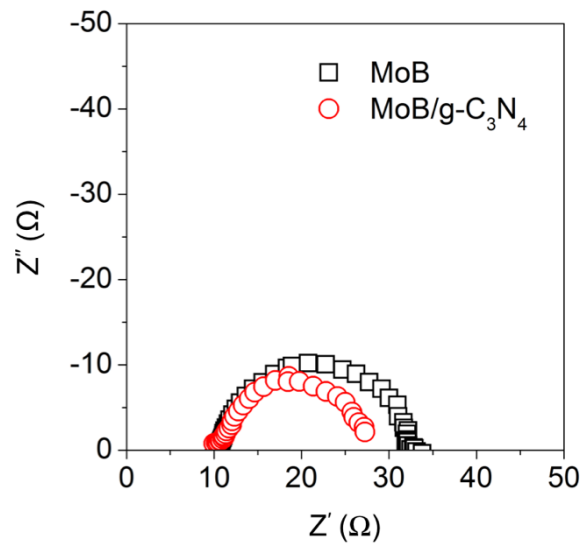


Figure S7. EIS plots of pure MoB and MoB/g-C₃N₄ Schottky catalyst.

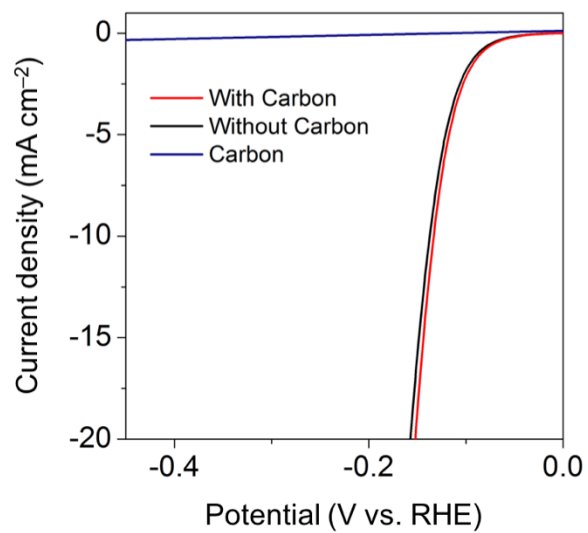


Figure S8. LSV polarization curves of MoB/g-C₃N₄ Schottky catalysts with or without carbon Vulcan XC72R in 1 M KOH.

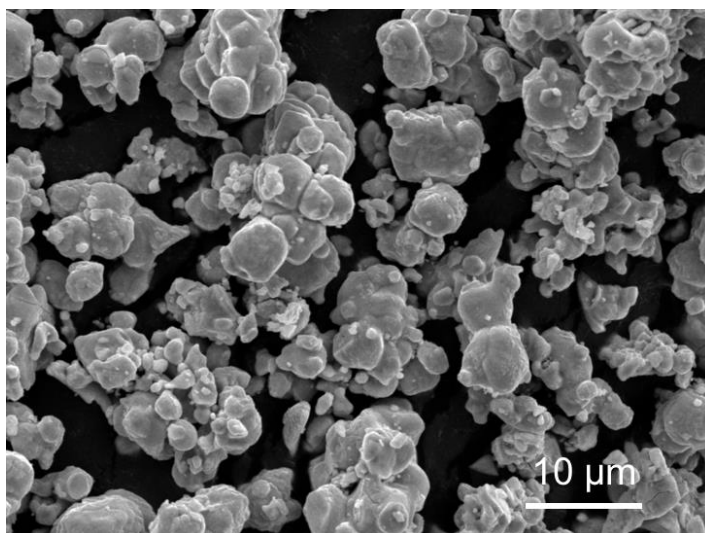


Figure S9. SEM image of hand-grinded MoB powder.

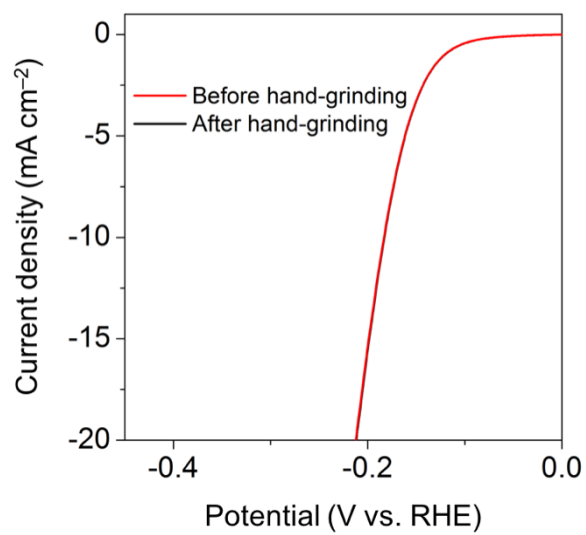


Figure S10. LSV polarization curves of MoB catalysts before or after hand-grinding in 1 M KOH.

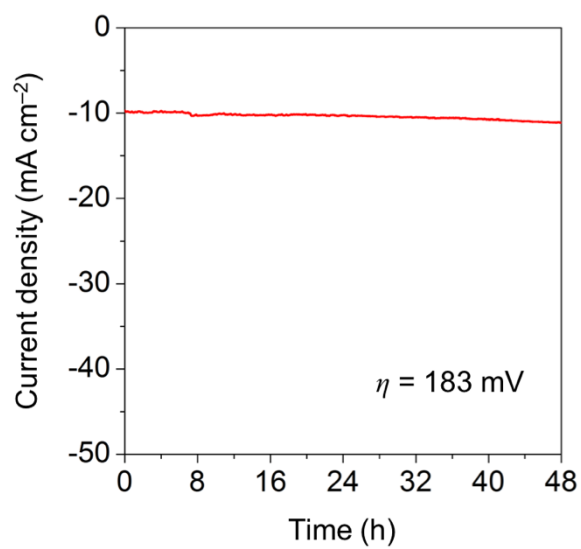


Figure S11. Chronoamperometric current–time ($i-t$) tests for pristine MoB powder.

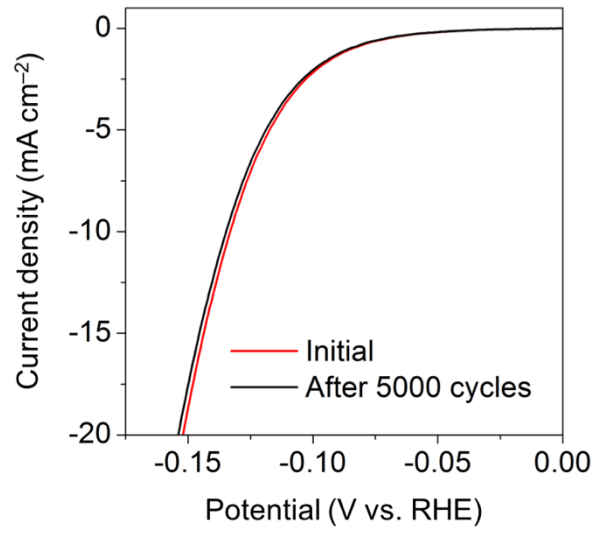


Figure S12. LSV polarization curves of MoB/g-C₃N₄ Schottky catalyst before and after 5000 cycles.

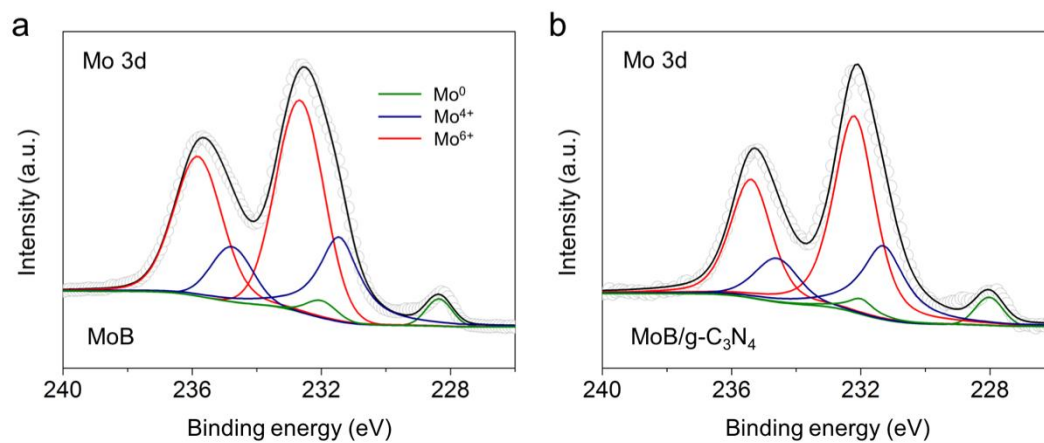


Figure S13. Mo 3d XPS spectra of (a) pristine MoB and (b) MoB/g-C₃N₄ Schottky catalyst.

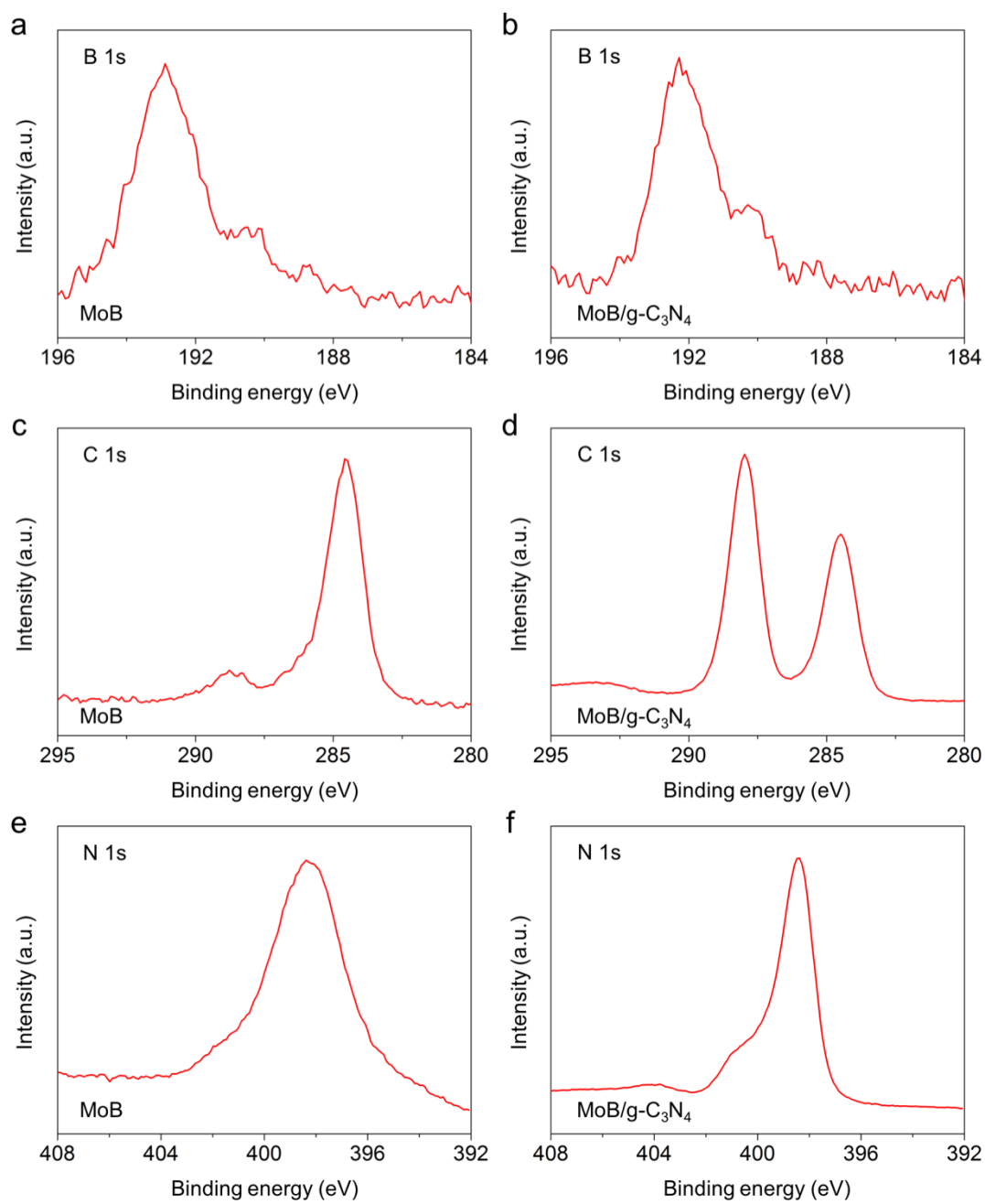


Figure S14. B 1s, C 1s and N 1s XPS spectra of pristine (a, c, e) MoB and (b, d, f) MoB/g-C₃N₄ Schottky catalyst.

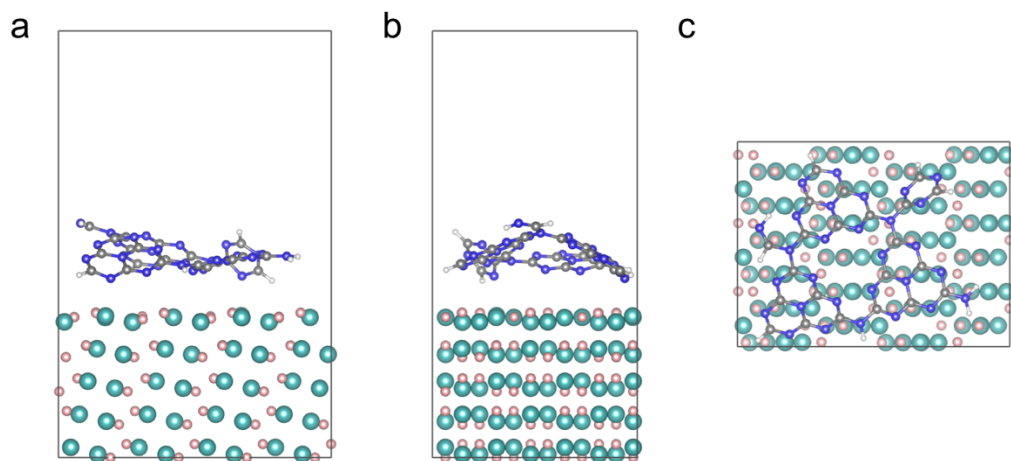


Figure S15. Side views (a, b) and top view (c) of the optimized geometry of MoB(112)/g-C₃N₄ Schottky catalyst.

Table S1. HER activities of MoB/g-C₃N₄ Schottky catalyst and recently reported most active noble metal-free catalysts in 1 M KOH electrolyte.

Catalysts	η_{onset} (mV)	η (mV) at 10 mA/cm ²	Tafel slope (mV/dec)
MoB/g-C₃N₄	40	133	46
α -MoB ^[7]	150	220	59
MoP ^[8]	50	130	48
MoC _x ^[9]	80	151	59
MoO _x /Ni ₃ S ₂ ^[10]	80	106	90
MoS ₂ /Ni ₃ S ₂ ^[11]	50	110	83
Co@N-doped CNTs ^[12]	140	370	69
CoSe ₂ ^[13]	80	200	85
CoP ^[14]	150	240	129
Co ₂ P ^[15]	15	60	40
CoP film ^[16]	20	94	42
Co(OH) ₂ /PANI ^[17]	50	90	92
Co@Co ₃ O ₄ ^[18]	30	95	44
NiCoP/rGO ^[19]	138	209	124
Ni ₈ P ₃ /Ni ^[20]	70	130	59
Ni ₈ S ₈ /Ni ^[20]	120	230	123
NiO/Ni-CNT ^[21]	0	80	82
Ni ₃ FeN ^[22]	160	158	42
Ni _{0.33} Co _{0.67} S ₂ ^[23]	50	88	118
NiCo ₂ O ₄ ^[24]	50	110	50

Table S2. Brunauer–Emmett–Teller (BET) surface area and electrochemical surface area (ECSA) of MoB/g-C₃N₄ Schottky catalysts with different weight ratios.

	MoB	MoB/g-C ₃ N ₄ -5:1	MoB/g-C ₃ N ₄ -3:1	MoB/g-C ₃ N ₄ -2:1	MoB*
BET (m ² g ⁻¹)	3.46	3.12	3.51	3.85	3.37
ECSA (μF cm ⁻²)	40	56	89	32	41

* The sample was hand-grinded for 0.5 h in an agate mortar before the measurements.

References

- [1] J. Vande Vondele, M. Krack, F. Mohamed, M. Parrinello, T. Chassaing, J. Hutter, *Comput. Phys. Commun.* **2005**, *167*, 103–128.
- [2] a) S. Nosé *J. Chem. Phys.* **1984**, *81*, 511–519; b) W. G. Hoover, *Phys. Rev. A* **1985**, *31*, 1695.
- [3] a) J. P. Perdew, *Phys. Rev. B* **1986**, *33*, 8822–8824; b) J. P. Perdew, K. Burke, M. Ernzerhof, *Phys. Rev. Lett.* **1996**, *77*, 3865–3868.
- [4] S. Grimmea, J. Antony, S. Ehrlich, H. Krieg, *J. Chem. Phys.* **2010**, *132*, 154104.
- [5] S. Goedecker, M. Teter, J. Hutter, *Phys. Rev. B* **1996**, *54*, 1703.
- [6] G. Henkelman, H. Jónsson, *J. Chem. Phys.* **2000**, *113*, 9978.
- [7] H. Vrubel, X. Hu, *Angew. Chemie - Int. Ed.* **2012**, *51*, 12703–12706.
- [8] P. Xiao, M. A. Sk, L. Thia, X. Ge, R. J. Lim, J.-Y. Wang, K. H. Lim, X. Wang, *Energy Environ. Sci.* **2014**, *7*, 2624–2629.
- [9] H. Bin Wu, B. Y. Xia, L. Yu, X.-Y. Yu, X. W. Lou, *Nat. Commun.* **2015**, *6*, 6512.
- [10] Y. Wu, G. Li, Y. Liu, L. Yang, X. Lian, T. Asefa, X. Zou, *Adv. Funct. Mater.* **2016**, *26*, 4839.
- [11] J. Zhang, T. Wang, D. Pohl, B. Rellinghaus, R. Dong, S. Liu, X. Zhuang, X. Feng, *Angew. Chemie- Int. Ed.* **2016**, *128*, 6814–6819.
- [12] X. Zou, X. Huang, A. Goswami, R. Silva, B. R. Sathe, T. Asefa, *Angew. Chemie - Int. Ed.* **2014**, *126*, 4461–4465.
- [13] P. Chen, K. Xu, S. Tao, T. Zhou, Y. Tong, H. Ding, L. Zhang, W. Chu, C. Wu, Y. Xie, *Adv. Mater.* **2016**, *28*, 7527–7532.
- [14] J. Tian, Q. Liu, A. M. Asiri, X. Sun, *J. Am. Chem. Soc.* **2014**, *136*, 7587–7590.
- [15] Y. Tan, H. Wang, P. Liu, C. Cheng, F. Zhu, A. Hirata, M. Chen, *Adv. Mater.* **2016**, *28*, 2951–2955.
- [16] N. Jiang, B. You, M. Sheng, Y. Sun, *Angew. Chemie - Int. Ed.* **2015**, *54*, 6251–6254.
- [17] J. X. Feng, L. X. Ding, S. H. Ye, X. J. He, H. Xu, Y. X. Tong, G. R. Li, *Adv. Mater.* **2015**, *27*, 7051–7057.
- [18] X. Yan, L. Tian, M. He, X. Chen, *Nano Lett.* **2015**, *15*, 6015–6021.
- [19] J. Li, M. Yan, X. Zhou, Z. Huang, Z. Xia, *Adv. Funct. Mater.* **2016**, *26*, 6785–6796.
- [20] G. Chen, T. Y. Ma, Z. Liu, N. Li, Y. Su, K. Davey, S. Qiao, *Adv. Funct. Mater.* **2016**, *26*, 3314–3323.
- [21] M. Gong, W. Zhou, M. Tsai, J. Zhou, M. Guan, M. Lin, B. Zhang, Y. Hu, D. Wang, J. Yang, et al., *Nat. Commun.* **2014**, *5*, 4695.
- [22] X. Jia, Y. Zhao, G. Chen, L. Shang, R. Shi, X. Kang, G. I. N. Waterhouse, L. Wu, C. Tung, T. Zhang, *Adv. Energ. Mater.* **2016**, *6*, 1502585.
- [23] Z. Peng, D. Jia, A. M. Al-enizi, A. A. Elzatahry, G. Zheng, *Adv. Energ. Mater.* **2015**, *5*, 1402031.
- [24] X. Gao, H. Zhang, Q. Li, X. Yu, Z. Hong, X. Zhang, C. Liang, Z. Lin, *Angew. Chemie - Int. Ed.* **2016**, *55*, 1–6.